

# On the interpretation of *SKS* splitting measurements in the presence of several layers of anisotropy

Barbara Romanowicz and Huaiyu Yuan

Seismological Laboratory, University of California at Berkeley, Berkeley, CA 94720, USA. E-mail: barbara@seismo.berkeley.edu

Accepted 2011 November 14. Received 2011 November 13; in original form 2011 June 7

## SUMMARY

Concerns over the validity of expressions derived by Montagner *et al.* that link *SKS* splitting measurements to the variation with depth of anisotropic parameters in the upper mantle have been recently expressed, pointing out that the long period approximations applied by these authors may not be valid for the frequency range commonly used in *SKS* studies, and in particular, that the anisotropy splitting parameters should depend on the order in which different anisotropy layers are arranged with depth. We show here that indeed, measurements of splitting time and fast axis direction performed at individual azimuths do depend on the order of layering, however, the expressions of Montagner *et al.* concern station-averaged quantities that do not depend on the order of layers. It is therefore correct to use these expressions in joint inversions of surface waveforms and *SKS* station-averaged splitting measurements. On the other hand, the depth-dependent sensitivity of surface waveforms naturally provides constraints on the order of layering. Having clarified this confusion, we extend the expressions of Montagner *et al.* to the case of a tilted axis of symmetry and non-vertical incident waves, and show that station-averaged estimates of ‘effective’ splitting parameters: splitting time, fast axis direction and tilt of the fast axis, can be related to the integral with depth of quantities, which now depend not only on the local splitting time and fast axis direction, but also on the local tilt of the fast axis, thus providing constraints also on the variation of the tilt with depth. We show that the effective parameters used as constraints in the inversion can be obtained either from the measurement of splitting intensity, or through a parameter search and cross-convolution method. In particular, in the case when the effective tilt is significant, the splitting intensity no longer presents 180° periodicity with azimuth, providing a diagnostic tool for the presence of such tilts in the upper mantle. Thus, combining body-wave and surface wave observations also has the potential of constraining the variation with depth of the tilt of the fast axis of anisotropy, a geodynamically important parameter.

**Key words:** Body waves; Surface waves and free oscillations; Seismic anisotropy; Seismic tomography; Theoretical seismology.

## 1 INTRODUCTION

The presence of seismic anisotropy in the upper mantle was discovered in the 1960s (e.g. Anderson 1961; Hess 1964). It has been confirmed in numerous studies since, and attributed to strain-induced lattice preferred orientation (LPO) of highly anisotropic minerals such as olivine, due to either present day flow, or ‘frozen’ flow from the geological past. In the last 20 yr, attention has focused primarily on two types of seismic measurements that are diagnostic of the presence of shear wave anisotropy in the upper mantle, the splitting of *SKS* waves and surface wave anisotropy. The latter manifests itself in two ways: (1) polarization anisotropy resulting from the discrepancy in Love- and Rayleigh-wave dispersion measurements (e.g. Schlue & Knopoff 1977) or toroidal and spheroidal

mode eigenfrequencies (e.g. Dziewonski & Anderson 1981), and (2) azimuthal anisotropy (e.g. Forsyth 1975). Surface wave anisotropy can be described by 13 elastic parameters (e.g. Montagner & Nataf 1986) of which five [the ‘Love’ parameters A,C,F,L,N; Love (1911)] correspond to a transversely isotropic medium with vertical axis of symmetry that gives rise to polarization anisotropy, and the other eight parameters enter in the description of azimuthal variations of surface wave phase velocities. Theoretical expressions relating the anisotropic elastic tensor  $C_{ij}$  to surface wave observations have been developed in the asymptotic limit by Smith & Dahlen (1973). In practice, only two transverse isotropy parameters (L,N) can be resolved reliably from long-period surface wave measurements, while the best resolved terms in azimuthal anisotropy are the  $2\Psi$  terms  $G_c$  and  $G_s$  (Montagner & Nataf 1986), where  $\Psi$  is azimuth.

Several global 3-D shear velocity models of the upper mantle have been developed at the global scale that include either transverse isotropy alone (e.g. Nataf *et al.* 1986; Ekström & Dziewonski 1998; Gung *et al.* 2003), or azimuthal anisotropy from the measurement of Rayleigh waves (e.g. Debayle & Kennett 2000; Debayle *et al.* 2005) or both radial and azimuthal anisotropy (e.g. Montagner & Tanimoto 1991; Montagner 2002). Many regional-scale anisotropic tomographic models of the upper mantle have also been published (e.g. Simons *et al.* 2002; Smith *et al.* 2004).

On the other hand, numerous methods have been developed to measure the fast axis direction and splitting time from *SKS* measurements at a single station under the assumption of one layer of anisotropy with a horizontal axis of symmetry (e.g. Vinnik *et al.* 1989; Silver & Chan 1991). These methods or variations thereof have been widely applied to many stations in the world (e.g. Silver 1996). Silver & Savage (1994) have shown evidence for the presence of multiple layers of anisotropy in different continents from observations of the azimuthal dependence of *SKS* splitting measurements. Theoretical expressions for the dependence of the measured splitting on the anisotropic parameters (fast axis direction, splitting time) of individual layers have been derived in several studies (e.g. Silver & Savage 1994; Rümpker & Silver 1998; Saltzer *et al.* 2000). In practice, such measurements are often difficult to interpret, since many other factors can affect single path observations of splitting. Chevrot & van der Hilst (2003) examined the influence of a dipping fast axis on splitting measurements.

Surface wave and body-wave measurements of upper-mantle anisotropy are somewhat complementary. Surface waves—especially if overtones are included—provide constraints on the depth dependence of anisotropy, but have poor lateral resolution. On the other hand, the lateral resolution of station-averaged *SKS* splitting measurements is as good as the distribution of available stations, but depth resolution is poorer. Chevrot (2006) have suggested that the use of finite frequency kernels for *SKS* splitting measurements can improve depth resolution using *SKS* splitting data alone.

Montagner *et al.* (2000) have shown how to relate *SKS* and surface wave azimuthal anisotropy measurements, under the assumption of horizontal axis of symmetry, for a multilayered upper-mantle anisotropic model, and have pointed out that *SKS* splitting predictions from surface wave based azimuthally anisotropic tomographic models do not always match actual *SKS* splitting measurements, especially in continental areas.

In a previous study, we have used the theoretical framework of Montagner *et al.* (2000), hereafter referred to as MGL00, to develop a method to jointly invert three-component teleseismic long-period waveforms (including fundamental mode and overtone surface waves) and *SKS* splitting measurements, and constrain 3-D variations in radial and azimuthal anisotropy in the upper mantle. We have applied this approach to the north American continent (Marone & Romanowicz 2007; Marone *et al.* 2007) and have shown that significantly different fast axis directions are obtained in the lithosphere and in the asthenosphere under the north American craton. Moreover, we showed that including constraints from *SKS* splitting measurements in the inversion allows better resolution of the strength of anisotropy below the cratonic lithosphere–asthenosphere boundary, while not changing the fast axis directions or degrading the fit to surface waveforms. This is because surface waves alone cannot recover the full amplitude of the signal at depths greater than 250–300 km. In the asthenosphere, the fast axis direction aligns with the absolute plate motion (APM) as measured in the hotspot reference frame (Gripp & Gordon 2002) both under the

craton, at depths greater than 250 km, and, at shallower depths (80–200 km) in the tectonic western part of north America. More recently, we have confirmed these results in a higher resolution study (Yuan *et al.* 2011), and in addition, we have shown the presence of two distinct layers of anisotropy with different directions of fast axis in the lithosphere of the north American craton (Yuan & Romanowicz 2010). Our studies suggest, in particular, that azimuthal anisotropy is a powerful tool for detecting layering in the continental lithosphere.

Silver & Long (2011) have expressed concerns about the validity of the MGL00 theoretical expressions as used in joint surface wave and *SKS* splitting tomography, pointing out that these expressions are based on the assumption of commutativity of the splitting operator between layers, which is theoretically valid only in a low-frequency approximation (periods longer than about 10 s according to MGL00). Silver & Long (2011) argue that the non-commutative part of the splitting operator must be retained, given that typical shear wave splitting studies are conducted at dominant periods on the order of 8–12 s, which do not warrant the application of the low-frequency approximation. Therefore, caution must be used before applying the expressions of MGL00 in practice.

In this paper, we show that Silver & Long's (2011) interpretation of MGL00's expressions is incorrect. We clarify that the MGL00 expressions involve observables that are independent of azimuth, and that do not depend on the order of layers to second order in the small parameter  $\omega\delta t$ , where  $\omega$  is angular frequency and  $\delta t$  denotes splitting time. We illustrate this in a series of synthetic examples. We also generalize the expressions of MGL00 to the case of a tilted axis of symmetry as well as non-vertical incidence, and show two ways in which the corresponding station-averaged observables can be measured from single station observations of either direct *S* waves or *Ps* converted phases.

## 2 THEORETICAL FRAMEWORK: CASE OF VERTICAL INCIDENCE AND TRANSVERSE ISOTROPY WITH A HORIZONTAL SYMMETRY AXIS

We adopt the formalism of MGL00 and start with the expression obtained by these authors for the displacement  $\mathbf{u}_S^1(\mathbf{z}, t)$  at the top of a single anisotropic layer for a model of anisotropy with a horizontal axis of symmetry, and for a vertically incident *S* wave (eq. 9 of MGL00). In this case, the geometry reduces to a 2-D problem in the horizontal plane (Fig. 1).

$$\mathbf{u}_S^1(\mathbf{z}, t) = \begin{bmatrix} u_R^1 \\ u_T^1 \end{bmatrix} = \mathbf{e}^{i\omega t} \mathbf{R}_{W \rightarrow A} \mathbf{H}_1 \mathbf{R}_{A \rightarrow W} \begin{bmatrix} u_{R_0} \\ 0 \end{bmatrix}. \quad (1)$$

Here,  $u_R^1$  and  $u_T^1$  are, respectively, the radial and transverse component of displacement at the top of the anisotropic layer, and  $u_{R_0}$  is the amplitude of the incident purely radial displacement. The rotation matrices that allow the passage from the reference frame defined by the fast axis of anisotropy ('A') to the geographical reference frame ('G') or the wave reference frame ('W') defined by the longitudinal and transverse directions are such that

$$\mathbf{R}_{W \rightarrow A} = \mathbf{R}_{W \rightarrow G} \mathbf{R}_{G \rightarrow A} = \begin{bmatrix} \cos(\Psi'_1) & -\sin(\Psi'_1) \\ \sin(\Psi'_1) & \cos(\Psi'_1) \end{bmatrix} = \mathbf{R}_1 \quad (2)$$

and

$$\mathbf{R}_{A \rightarrow W} = \mathbf{R}_{W \rightarrow A}^{-1}. \quad (3)$$

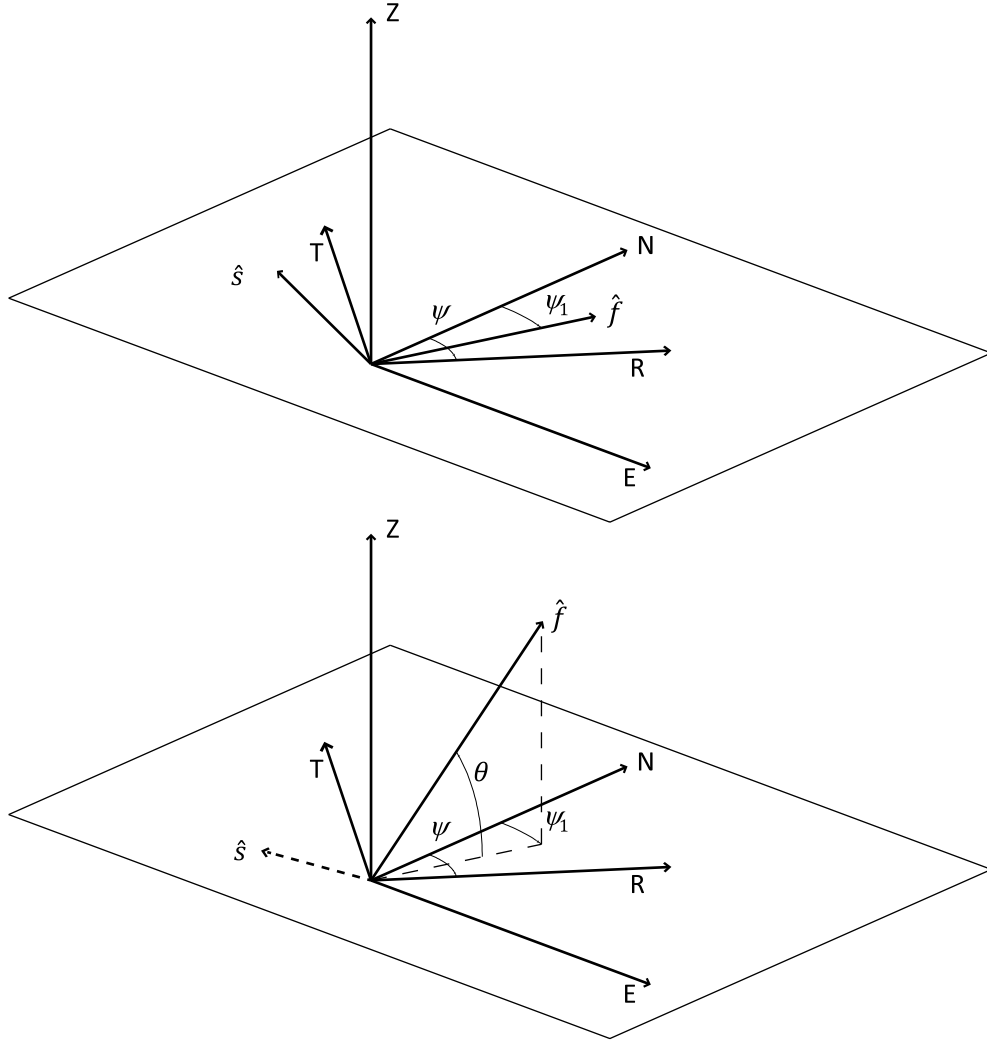


**Figure 1.** Definitions of angles used in this paper. (a) Case of anisotropy with a horizontal axis of symmetry and vertical propagation; (b) case of a tilted axis of symmetry.

Here  $\Psi$  is the azimuth from north of the ray path and  $\Psi_1$ , the azimuth from north of the fast axis direction, and  $\Psi'_1 = \Psi_1 - \Psi$ . Also, following MGL00

$$\mathbf{H}_1 = \begin{bmatrix} e^{i+} & 0 \\ 0 & e^{i-} \end{bmatrix}, \quad (4)$$

where

$$e^{i\pm} = \exp \left[ -i\omega \frac{z - z_0}{V_{S_0} \pm \delta V/2} \right] = \exp \left[ -i\omega \frac{z - z_0}{V_{S_0}} \right] \exp(\mp i\omega \delta t), \quad (5)$$

with  $\delta t = \frac{(z - z_0)\delta V}{V_{S_0}^2}$ ,  $z_0$  and  $V_{S_0}$  are the depth to the bottom of the anisotropic layer, and the isotropic velocity just below the layer, respectively.  $\delta V/V_{S_0}$  is the relative velocity difference between the fast and the slow waves in the anisotropic layer. Evaluating expression (1), we obtain

$$\begin{aligned} u_R^1(z, t) &= [\cos(\omega \delta t/2) + i \sin(\omega \delta t/2) \cos(2\Psi'_1)] u_R^0(t), \\ u_T^1(z, t) &= i \sin(\omega \delta t/2) \sin(2\Psi'_1) u_R^0(t). \end{aligned} \quad (6)$$

In particular, to second order in  $\omega \delta t$

$$u_T^1(z, t) = 0.5 \delta t \sin(2\Psi'_1) \dot{u}_R^0(t), \quad (7)$$

where  $\dot{u}_R^0(t)$  is the time derivative of  $u_R^0(t)$ . This is the same expression as obtained by Vinnik *et al.* (1989), Silver & Chan (1991) and many other authors. It forms the basis of many commonly used methods for the measurement of splitting parameters from SKS waveform data.

Following MGL00, we can generalize eq. (6) to the case of multiple layers. In the case of two layers, the displacement vector at the top of the second layer is

$$\mathbf{u}_S^2(\mathbf{z}, \mathbf{t}) = \begin{bmatrix} u_R^2 \\ u_T^2 \end{bmatrix} = \mathbf{e}^{i\omega \mathbf{t}} \mathbf{R}_2 \mathbf{H}_2 \mathbf{R}_2^{-1} \mathbf{u}_S^1(\mathbf{z}, \mathbf{t}), \quad (8)$$

where the indices refer to the respective layers. We introduce the notation, as in Silver & Long (2011)

$$\theta_i = \omega \delta t_i/2, \quad (9)$$

and

$$\begin{aligned} a_p &= \cos(\theta_2)\cos(\theta_1) - \sin(\theta_2)\sin(\theta_1)\cos 2(\Psi_2 - \Psi_1), \\ C_c &= \cos(\theta_1)\sin(\theta_2)\cos 2\Psi'_2 + \cos(\theta_2)\sin(\theta_1)\cos 2\Psi'_1, \\ a_{p\perp} &= -\sin(\theta_2)\sin(\theta_1)\sin 2(\Psi_2 - \Psi_1), \\ C_s &= \cos(\theta_1)\sin(\theta_2)\sin 2\Psi'_2 + \cos(\theta_2)\sin(\theta_1)\sin 2\Psi'_1 \end{aligned} \quad (10)$$

Evaluating eq. (8), we obtain, without any further approximation,

$$\begin{aligned} u_R^2 &= [a_p + iC_c]u_{R_0}, \\ u_T^2 &= [a_{p\perp} + iC_s]u_{R_0}. \end{aligned} \quad (11)$$

It is straightforward to see that these expressions are the same ones as in Silver & Savage (1994) and Silver & Long (2011) where the parameter  $\alpha_i$  used by these authors is here  $\alpha_i = 2\Psi'_i$ , which, we stress, depends on the azimuth at which the displacement is calculated.

By comparing eq. (11) to those obtained for a single ‘equivalent’ anisotropic layer with effective delay time  $\delta\hat{t}$  (evaluated for a single azimuth  $\Psi$ ) and apparent fast axis direction  $\hat{\Psi}$ , and without further approximations, following Silver & Long (2011), equating real and imaginary parts and eliminating  $u_{R_0}$  we obtain

$$\begin{aligned} \tan 2(\hat{\Psi} - \Psi) &= \frac{a_{p\perp}^2 + C_s^2}{C_c C_s + a_p a_{p\perp}}, \\ \tan\left(\frac{\omega\delta\hat{t}}{2}\right) &= \sqrt{\frac{(C_c C_s + a_p a_{p\perp})^2 + (a_{p\perp}^2 + C_s^2)^2}{(a_p C_s - C_c a_{p\perp})^2}}. \end{aligned} \quad (12)$$

The long period approximation of eq. (12) is (Silver & Long 2011)

$$\begin{aligned} \tan 2(\hat{\Psi} - \Psi) &= \frac{C_s^2}{a_{p\perp} + C_s C_c}, \\ \tan\left(\frac{\omega\delta\hat{t}}{2}\right) &= \sqrt{[a_{p\perp}/C_s + C_c]^2 + C_s^2}. \end{aligned} \quad (13)$$

Through the dependence of  $a_{p\perp}$  on  $\sin 2(\Psi_2 - \Psi_1)$ , expressions (12) and (13) do indeed depend on the order of the layers. They are valid to second order in  $\omega\delta t$ .

Silver & Long (2011) mistakenly claim however that, in applying a long period approximation, MGL00 set to zero the term  $a_{p\perp}$  in expressions (13) to obtain effective splitting parameters that do not depend on the order of layers. This statement is incorrect, because neither MGL00, nor we (Marone & Romanowicz 2007; Yuan & Romanowicz 2010) actually use eq. (13) at any point. We note that these expressions depend on the azimuth  $\Psi$  and are therefore valid for measurements at a particular azimuth  $\Psi$ . As we will show in synthetic examples, it is, in fact, not wise to apply any long period approximations at all to expressions (12), which involve divisions by quantities that can tend to zero in the vicinity of specific values of the azimuth  $\Psi$ . In contrast, expressions (21) and (22) in MGL00 are obtained without division by quantities which depend on the azimuth, and these expressions directly give the effective azimuthally averaged splitting time  $\delta\hat{t}$  and fast axis direction  $\hat{\Psi}$ .

To show this more explicitly, let us go back to eq. (8), and first generalize them to the case of  $n$  layers, evaluated to second order in  $\omega\delta t$ , that is, the same order of approximation as used in deriving expressions (13). After some algebra, we obtain the compact

expressions:

$$\begin{aligned} u_R^n &= u_{R_0} + \sum_{i=1}^{i=n} \left[ \frac{i\omega\delta t_i}{2} \cos 2\Psi'_i \right] u_{R_0} - \omega^2 \\ &\quad \times \left[ \sum_i \sum_{j>i} \frac{\delta t_i}{2} \frac{\delta t_j}{2} \cos 2(\Psi_j - \Psi_i) \right] u_{R_0}, \\ u_T^n &= \sum_{i=1}^{i=n} \left[ \frac{i\omega\delta t_i}{2} \sin 2\Psi'_i \right] u_{R_0} - \omega^2 \\ &\quad \times \left[ \sum_i \sum_{j>i} \frac{\delta t_i}{2} \frac{\delta t_j}{2} \sin 2(\Psi_j - \Psi_i) \right] u_{R_0}, \end{aligned} \quad (14)$$

where

$$\delta t_i = \frac{(z_i - z_{i-1})\delta V_i}{V_{S_i}^2}. \quad (15)$$

Here  $i, j$  denote the indices of the different layers of anisotropy. We note that, indeed, to this order of approximation, the expression for  $u_T^n$  depends on the order of the layers, through the sign of the  $\sin 2(\Psi_j - \Psi_i)$  term. Notably, this term does not depend on the azimuth.

Now, instead of solving directly for the effective splitting time and fast axis direction, as done in Silver & Long (2011), which leads to potential instabilities due to division by small numbers, we reiterate that  $\Psi'_i$  depends on the azimuth  $\Psi$  and note that we can write the azimuthal dependence of expression (14) in the form

$$u_T^n = A \cos 2\Psi + B \sin 2\Psi + C, \quad (16)$$

where, assuming  $u_{R_0}$  and its time derivatives do not depend on azimuth (we have assumed vertical incidence), to second order in  $\omega\delta t$ .

$$\begin{aligned} A &= \sum_i \sin(2\Psi_i) \frac{\delta t_i}{2} \ddot{u}_{R_0}, \\ B &= -\sum_i \cos(2\Psi_i) \frac{\delta t_i}{2} \ddot{u}_{R_0}, \\ C &= \sum_{j>i} \frac{\delta t_i}{2} \frac{\delta t_j}{2} \sin 2(\Psi_j - \Psi_i) \ddot{u}_{R_0}. \end{aligned} \quad (17)$$

We can compare eq. (17) to the same order expressions obtained for an equivalent one layer model with ‘effective’ splitting time  $\delta\hat{t}$  and fast axis direction  $\hat{\Psi}$  (eq. 6).

$$\begin{aligned} A &= \sin(2\hat{\Psi}) \frac{\delta\hat{t}}{2} \ddot{u}_{R_0}, \\ B &= -\cos(2\hat{\Psi}) \frac{\delta\hat{t}}{2} \ddot{u}_{R_0}, \\ C &= 0. \end{aligned} \quad (18)$$

Thus, replacing the summation over layers by an integral (as in MGL00), we obtain the following expressions relating the ‘effective’ splitting time and fast axis direction (which are now independent of azimuth) to those in the individual layers, valid to second order in  $\omega\delta t$ :

$$\begin{aligned} \sin(2\hat{\Psi}) \frac{\delta\hat{t}}{2} &= \int_0^a \frac{\delta V_S(z)}{V_S^2(z)} \sin 2\Psi_G(z) dz, \\ \cos(2\hat{\Psi}) \frac{\delta\hat{t}}{2} &= \int_0^a \frac{\delta V_S(z)}{V_S^2(z)} \cos 2\Psi_G(z) dz, \end{aligned} \quad (19)$$

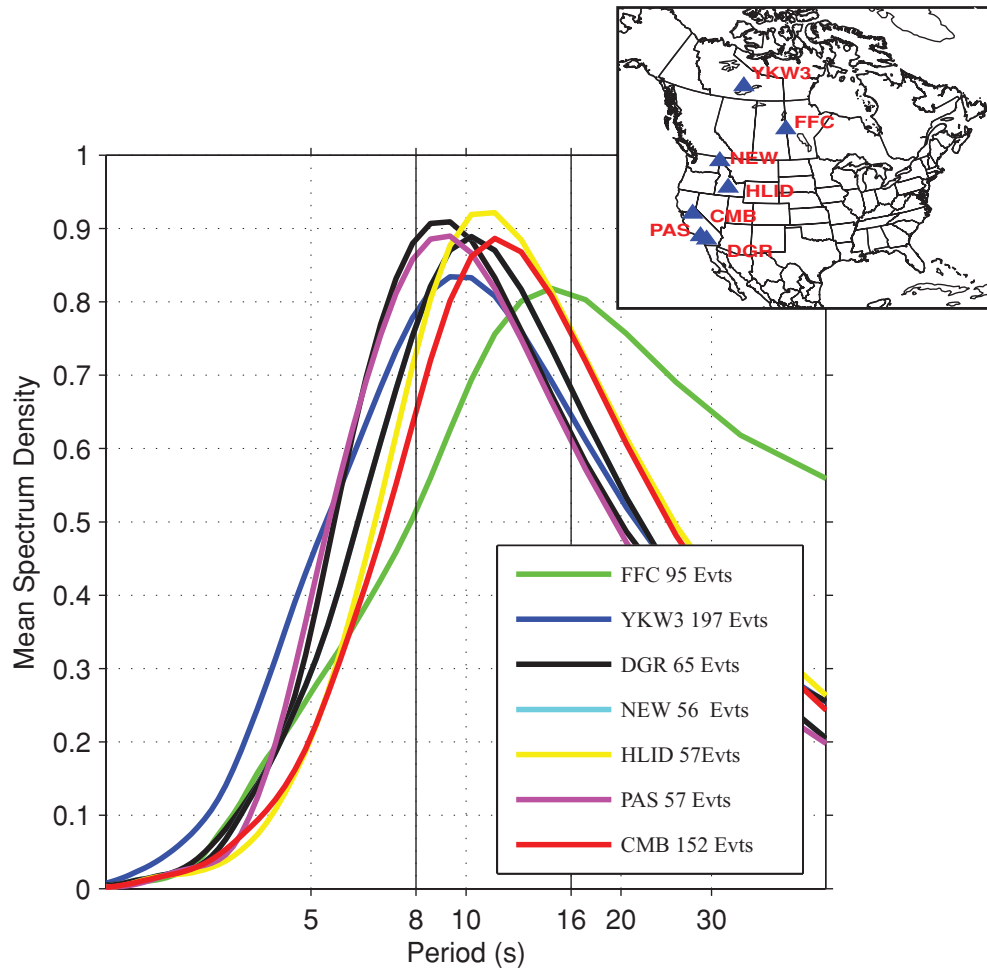


**Figure 2.** SKS radial component waveform spectra for selected permanent stations. For each station, the characteristic peak period is estimated from the averaged spectral density functions from multiple events. The number of events for each estimate is indicated. Inset shows the station locations.

where  $\Psi_G(z)$  is the direction of the fast axis at depth  $z$ . Noting the identity  $\delta V_s/V_s = G/L$ , where  $G$  and  $L$  are the anisotropic parameters of the model at depth  $z$  (MGL00), these are exactly expressions (21) and (22) of MGL00.

These expressions, used in Marone & Romanowicz (2007) and in Yuan & Romanowicz (2010) and Yuan *et al.* (2011), do not depend on the order of the anisotropic layers, and are valid to second order in  $\omega\delta t$ . The only term in eq. (14) which depends on the order of layers is independent of azimuth and therefore enters into the definition of the term  $C$ . So, when computing the station-averaged effective splitting parameters using a robust method that considers observations in a large enough range of azimuths, the only difference with the ‘pure’ one layer case is a constant shift term ( $C$ ) of second order.

In Marone & Romanowicz (2007) and Yuan & Romanowicz (2010), we used station-averaged splitting parameters. We considered tabulated values of  $\delta t$  and  $\hat{\Psi}$  taken from the literature. As discussed in our papers, we rely on them being robust. On the other hand, we do not need separate measurements of these two splitting parameters, only of the products  $\delta t \sin(2\hat{\Psi})$  and  $\delta t \cos(2\hat{\Psi})$ , which can be obtained from measurements of the ‘splitting intensity’  $\delta t \sin(2(\hat{\Psi} - \Psi))$  as defined by Chevrot (2000) and advocated by Silver & Long (2011). The splitting intensity is a robust quantity independent of the order of layers that can be obtained by projecting the observed transverse component onto the radial component. The coefficients of the azimuthal expansion of the splitting intensity are,

in fact, what is used in Marone & Romanowicz (2007) and Yuan & Romanowicz (2010) and Yuan *et al.* (2011), with the only difference that we rely on station-averaged estimates of the splitting time and fast axis direction to form the products  $\delta t \sin(2\hat{\Psi})$  and  $\delta t \cos(2\hat{\Psi})$ , rather than on measurements of the splitting intensity, which are so far rarely reported in the literature.

As shown in Silver & Savage (1994) and in Silver & Long (2011), using splitting measurements at individual azimuths (i.e. for a given event/station pair) theoretically yields additional constraints on the order of layering. However, this type of measurement is rarely robust, due to the presence of noise. On the other hand, the depth sensitivity of surface waves down to 250–300 km of the upper mantle naturally provide constraints on the order of layering in the joint SKS/surface waveform inversion.

To illustrate the validity of using station-averaged measurements in expressions (19), we have carried out simple synthetic tests at two different periods, 8 s and 16 s, which cover the characteristic range of frequencies of SKS splitting measurements (e.g. Fig. 2). We consider the same four anisotropic models as described in Silver & Long (2011), shown in Fig. 3.

In Figs 4 (8 s) and 5 (16 s), we consider the same two layered models as described in Silver & Long (2011) and compare expressions (12) evaluated exactly and to second order in  $\omega\delta t$  (as in eq. 14). We also show for comparison the azimuth-independent effective splitting parameters obtained using the expressions of MGL00.



Model A	Model B
$\psi_1 = \text{N}135^\circ\text{E}, \delta t_1 = 1.0 \text{ s}$	$\psi_1 = \text{N}90^\circ\text{E}, \delta t_1 = 1.4 \text{ s}$
$\psi_2 = \text{N}90^\circ\text{E}, \delta t_2 = 1.4 \text{ s}$	$\psi_2 = \text{N}135^\circ\text{E}, \delta t_2 = 1.0 \text{ s}$
Model C	Model D
$\psi_1 = \text{N}135^\circ\text{E}, \delta t_1 = 0.5 \text{ s}$	$\psi_1 = \text{N}90^\circ\text{E}, \delta t_1 = 0.7 \text{ s}$
$\psi_2 = \text{N}90^\circ\text{E}, \delta t_2 = 0.7 \text{ s}$	$\psi_2 = \text{N}135^\circ\text{E}, \delta t_2 = 0.5 \text{ s}$

**Figure 3.** Simple two-layer anisotropic models used for synthetic tests. The fast axis direction ( $\Psi_i$ ) and delay time ( $\delta t_i$ ) is indicated for each layer. Model A consists of two anisotropic layers with large splitting times (1.0 and 1.4 s, respectively). Model B consists of the same two anisotropic layers as in Model A but the order of the layers is reversed. Models C and D are the same as Models A and B, respectively, except the splitting time in each layer is reduced by half. These are the same models as used in Silver & Long (2011).

Figs 4 and 5 show that, even the second-order approximation for the splitting time has a tendency to blow up in the vicinity of the azimuth that corresponds to very small values of the denominator in the second of eq. (12). The range of instability for the splitting time estimation is wider at shorter periods and for a model with stronger anisotropy (Fig. 4, top panels).

To reproduce more realistically measurements as they are done in practice, we have also computed noise-free synthetic waveforms using an anisotropic reflectivity code (Park 1996; Levin & Park 1997), with a near vertical incidence angle ( $3^\circ$ ) at the bottom of the anisotropic region, for all computations. The apparent splitting parameters for an equivalent one-layer model are measured on the synthetics for individual backazimuths ranging from  $0^\circ$  to  $180^\circ$  with  $10^\circ$  increments. Effective station-averaged parameters are also measured, assuming equal weight for each individual backazimuth. The cross-convolution method (Menke & Levin 2003; Yuan *et al.* 2008) is used in all measurements. The results are also shown in Figs 4 and 5. The splitting measurements for individual backazimuths match the analytical predictions for all models at both 8 s and 16 s period, validating our synthetic computational approach. Large misfits for the splitting time are found within the azimuth ranges where expressions (13) become close to singular.

Figs 4 and 5 clearly show the agreement between the predictions from the MGL00 expressions and the station-averaged splitting parameters, which are also summarized in Table 1. Small systematic shifts in the splitting times and fast axis directions are found between these two estimates. As indicated in eq. (17), the constant shift term (C) is of second order in  $\omega\delta t$ , therefore it is small, but shows larger departures from zero for models with large delay times (Models A and B) and at short periods. This is confirmed in Figs 4, 5 and Table 1. In all the cases tested, however, the agreement in splitting times and fast axis directions is well within the  $5\text{--}10^\circ$  and 0.2 s error bounds of typical *SKS* observations (e.g. Liu 2009). To further illustrate the agreement between the MGL00 predictions and the station averages, we combine the station-averaged measurements

$\delta\hat{t}$  and  $\hat{\Psi}$  to form the new parameter  $\delta\hat{t} \sin 2(\hat{\Psi} - \Psi)$  and plot it against backazimuth  $\Psi$  (Fig. 6). This new parameter is the splitting intensity of Chevrot (2000) (see also figs 3 and 5 in Silver & Long 2011). We also plot  $\delta\hat{t}$  and  $\hat{\Psi}$  as predicted by MGL00. It is clear that the curves in Fig. 6 are indistinguishable in practice, especially in the case of small delay times (Model C and D).

In our joint surface wave and *SKS* inversion (Marone & Romanowicz 2007; Yuan & Romanowicz 2010; Yuan *et al.* 2011) the typical vertical parametrization is on the order of 30–50 km in the shallow upper mantle, a small delay time within each anisotropic depth range is therefore generally warranted. We conclude that using expressions (19) as in (Marone & Romanowicz 2007; Yuan & Romanowicz 2010) is fully justified.

### 3 CASE OF NON-VERTICAL INCIDENCE AND TRANSVERSE ISOTROPY WITH A TILTED SYMMETRY AXIS

Expressions (1) and (2) can be generalized to the case of non-vertical incidence as well as tilted axis of symmetry in a hexagonal anisotropic model by introducing appropriate coordinate rotation matrices. Let  $\Theta_j$  and  $\Psi_j$  be the tilt from the horizontal plane, and azimuth from north, respectively, of the fast axis of anisotropy in layer  $j$ .

In this case, for each layer  $j$

$$R_{W \rightarrow A} = R_{W \rightarrow G} R_{G \rightarrow A} = \begin{bmatrix} \cos(\Psi'_j) & -\sin(\Psi'_j) & 0 \\ \sin(\Psi'_j) & \cos(\Psi'_j) & 0 \\ 0 & 0 & 1 \end{bmatrix} \times \begin{bmatrix} \cos(\Theta_j) & 0 & -\sin(\Theta_j) \\ 0 & 1 & 0 \\ \sin(\Theta_j) & 0 & \cos(\Theta_j) \end{bmatrix}. \quad (20)$$

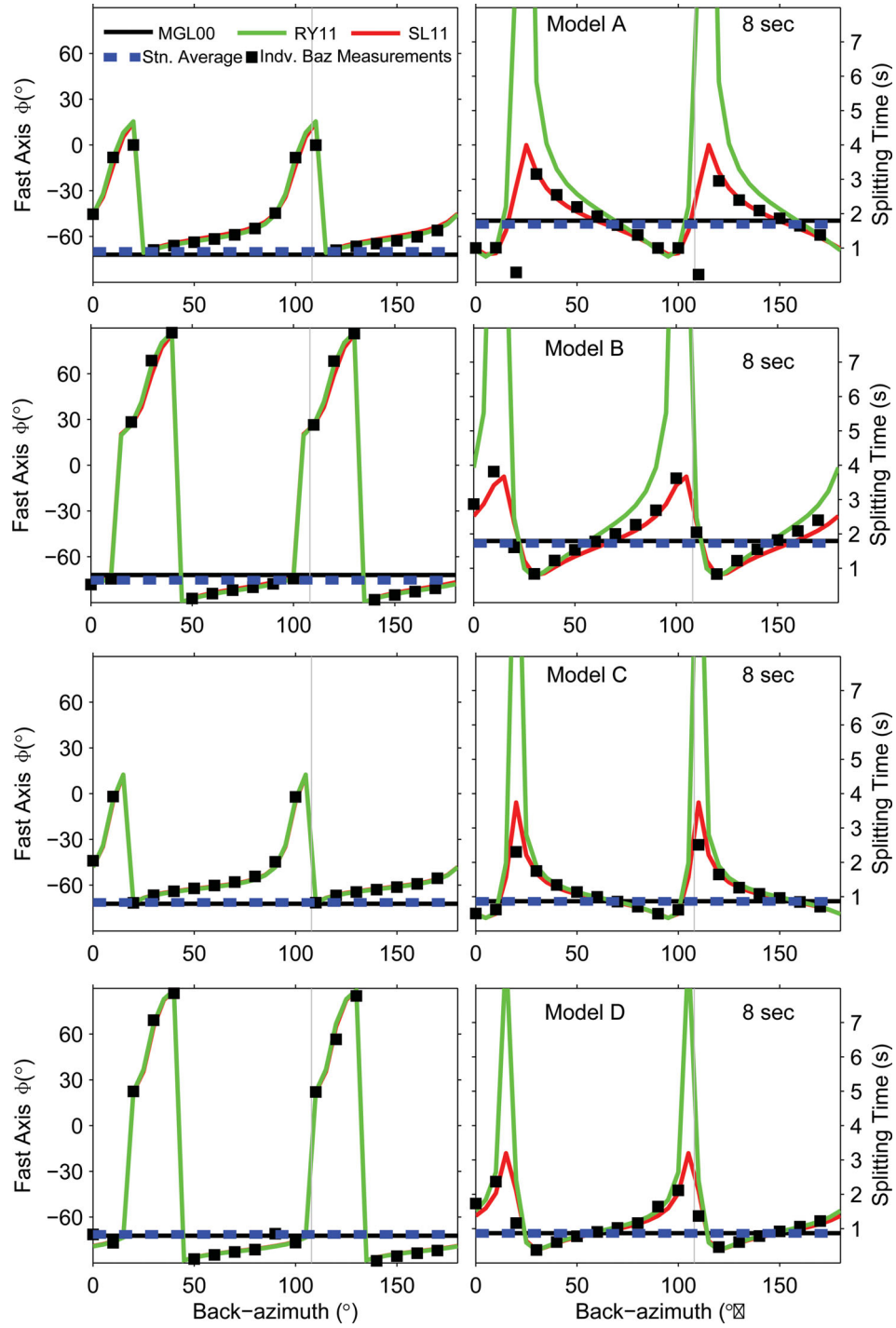


**Figure 4.** Comparison of apparent splitting parameters as a function of azimuth, at a period of 8 s, for models A–D (respectively from top to bottom). In the left-hand column are shown the splitting times, and in the right-hand column, the fast axis directions. Analytical predictions are shown by continuous lines, and measurements on synthetic waveforms by symbols. Red line: calculation using eq. (12) (Silver & Long 2011); Green line: calculation using the two-layer equivalent of eq. (14); black line: azimuth independent expression of MGL00. Black squares: measurements at individual azimuths; blue rectangles: station-averaged measurements.

Eq. (1) becomes, for the first layer

$$\mathbf{u}_S^1(\mathbf{z}, \mathbf{t}) = \begin{bmatrix} u_R^1 \\ u_T^1 \\ u_Z^1 \end{bmatrix} = \mathbf{e}^{i\omega t} \mathbf{R}_1 \mathbf{H}_1 \mathbf{R}_1^{-1} \begin{bmatrix} u_R^0 \\ u_T^0 \\ u_Z^0 \end{bmatrix}, \quad (21)$$

where we now need to consider the initial displacement on all three

components, as well as the final displacement on the vertical component. For the  $j$ th layer, we obtain

$$\mathbf{u}_S^j(\mathbf{z}, \mathbf{t}) = \mathbf{e}^{i\omega t} \mathbf{R}_{j-1} \mathbf{H}_{j-1} \mathbf{R}_{j-1}^{-1} \begin{bmatrix} u_R^{j-1} \\ u_T^{j-1} \\ u_Z^{j-1} \end{bmatrix}, \quad (22)$$

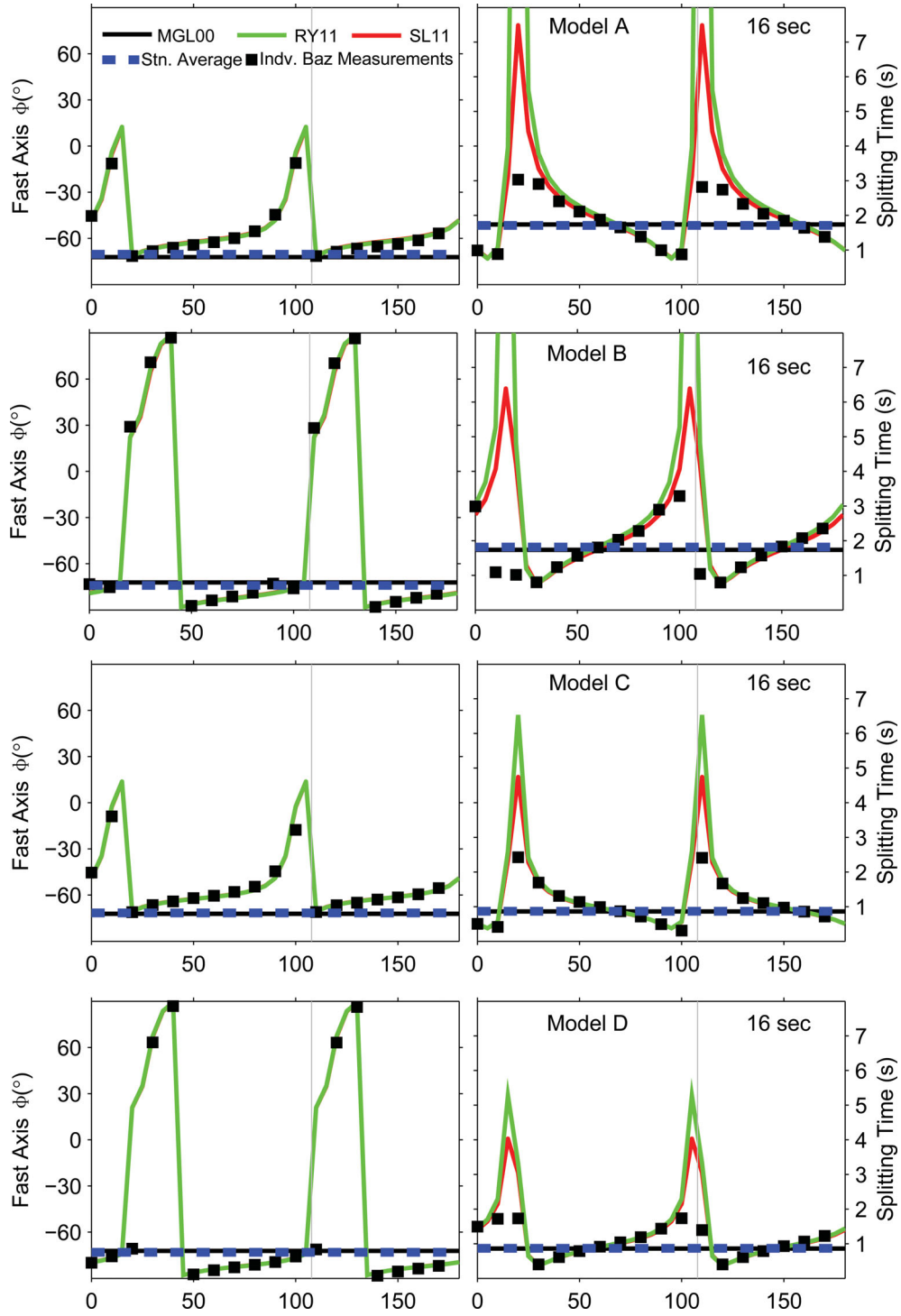


**Figure 5.** Same as Fig. 4 but for the period of 16 s. Note in the case of small splitting times and low frequency (Model C and D), the second-order approximation gives very close predictions compared with the equations with full terms and of Silver & Savage (1994).

where

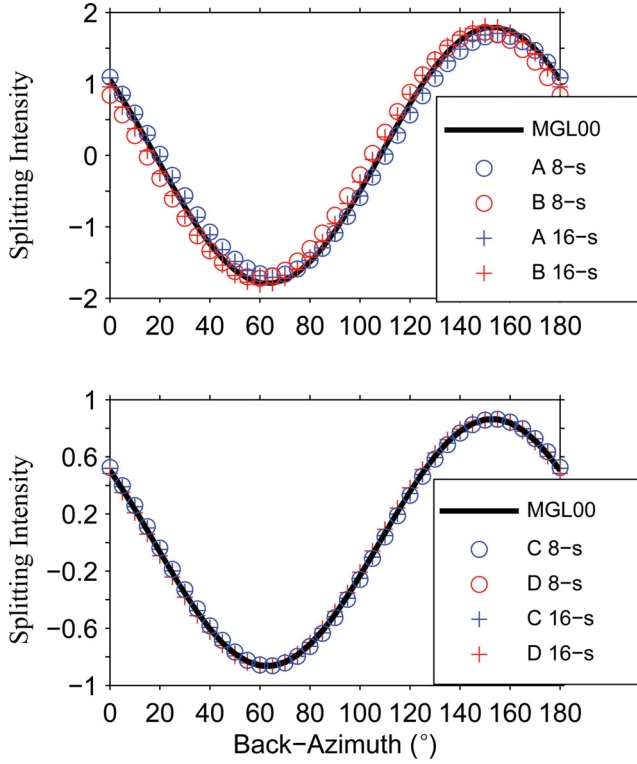
$$H^{j-1} = \begin{bmatrix} e_{j-1}^{i+} & 0 \\ 0 & e_{j-1}^{i-} \\ 0 & 0 & e_{j-1}^{i-} \end{bmatrix}. \quad (23)$$

After some algebra, we obtain, to first order in  $\omega\delta t$ , for an  $S$  wave of incidence angle  $I$  at the bottom of a stack of  $n$  anisotropic layers, each with fast axis direction defined by its azimuth from north  $\psi_j$  and tilt from horizontal by an angle  $\Theta_j$  and time-shift  $\delta t_j$  as defined in (15).



**Table 1.** First-order term predictions and station-averaged splitting parameters from synthetic measurements.

	Model A ( $\hat{\Psi}$ , $\delta t$ )	Model B ( $\hat{\Psi}$ , $\delta t$ )	Model C ( $\hat{\Psi}$ , $\delta t$ )	Model D ( $\hat{\Psi}$ , $\delta t$ )
Prediction using first-order term	( $-72.2^\circ$ , 1.72 s)	( $-72.2^\circ$ , 1.72 s)	( $-72.2^\circ$ , 0.86 s)	( $-72.2^\circ$ , 0.86 s)
Measured 8 s station average	( $-69.8^\circ$ , 1.68 s)	( $-75.4^\circ$ , 1.72 s)	( $-71.3^\circ$ , 0.86 s)	( $-71.3^\circ$ , 0.86 s)
Measured 16 s station average	( $-70.3^\circ$ , 1.71 s)	( $-74.1^\circ$ , 1.81 s)	( $-71.6^\circ$ , 0.87 s)	( $-73.0^\circ$ , 0.87 s)

**Figure 6.** The measured synthetic station-averaged splitting times  $\delta \hat{t}$  and fast axis directions  $\hat{\Psi}$ , are combined into a new parameter  $\delta t \sin 2(\Psi - \hat{\Psi})$ , that is, the ‘splitting intensity’ (Chevrot 2000), and plotted as circles and pluses against individual backazimuths. In the top panel, blue circles and crosses are for the 8 s and 16 s synthetics for Model A, and red circles and crosses, 8 s and 16 s for Model B. The bottom panel shows the case of Models C and D. The measured values are in good agreement with the predictions from the expressions of MGL00 recombined into the ‘splitting intensity’ (black line).

$$\begin{aligned}
u_R^n &= u_R^0 + \sum_{j=0}^n \frac{i\omega\delta t_j}{2} [(\cos 2\Psi_j \cos^2 \Theta_j - \sin^2 \Theta_j) u_R^0 \\
&\quad + \cos \Psi_j \sin 2\Theta_j u_Z^0 + u_T^0 \sin 2\Psi_j \cos^2 \Theta_j], \\
u_T^n &= u_T^0 + \sum_{j=0}^n \frac{i\omega\delta t_j}{2} [\cos^2 \Theta_j \sin 2\Psi_j u_R^0 \\
&\quad + \sin 2\Theta_j \sin \Psi_j u_Z^0 - u_T^0 (\sin^2 \Theta_j + \cos^2 \Theta_j \cos 2\Psi_j)], \\
u_Z^n &= u_Z^0 + \sum_{j=0}^n \frac{i\omega\delta t_j}{2} [\sin 2\Theta_j \cos \Psi_j u_R^0 - \cos 2\Theta_j u_Z^0 \\
&\quad + u_T^0 \sin 2\Theta_j \sin \Psi_j],
\end{aligned} \tag{24}$$

where the initial amplitude at the bottom of the anisotropic stack is

$$\begin{bmatrix} u_R^0 \\ u_T^0 \\ u_Z^0 \end{bmatrix} = \begin{bmatrix} a_0 \cos I \\ u_T^0 \\ a_0 \sin I \end{bmatrix}. \tag{25}$$

By the same type of analysis as for the simpler case of a horizontal axis of symmetry, we can obtain constraints on the parameters of anisotropy by developing  $u_T^n$  and  $u_R^n$  in harmonic components of the azimuth  $\Psi$  (to first order), taking into account the relation between  $u_R^0$  and  $u_Z^0$  from eq. (25).

$$\begin{aligned}
u_T &= A \cos 2\Psi + B \sin 2\Psi + A_1 \cos \Psi + B_1 \sin \Psi + C, \\
u_R &= D \cos 2\Psi + E \sin 2\Psi + D_1 \cos \Psi + E_1 \sin \Psi + F,
\end{aligned} \tag{26}$$

where

$$\begin{aligned}
A &= i\omega \sum_{j=0}^n \frac{\delta t_j}{2} [\cos^2 \Theta_j \sin 2\Psi_j u_R^0 - \cos^2 \Theta_j \cos 2\Psi_j u_T^0], \\
B &= -i\omega \sum_{j=0}^n \frac{\delta t_j}{2} [\cos^2 \Theta_j \cos 2\Psi_j u_R^0 - \cos^2 \Theta_j \sin 2\Psi_j u_T^0], \\
A_1 &= i\omega \sum_{j=0}^n \frac{\delta t_j}{2} \sin 2\Theta_j \sin \Psi_j u_R^0 \tan I, \\
B_1 &= -i\omega \sum_{j=0}^n \frac{\delta t_j}{2} \sin 2\Theta_j \cos \Psi_j u_R^0 \tan I, \\
C &= u_T^0 \left( 1 - \frac{i\omega\delta t_j}{2} \sin^2 \Theta_j \right).
\end{aligned} \tag{27}$$

Assuming the initial radial component  $u_R^0$  has little variation with azimuth, we obtain similar equations to the case of a horizontal axis of symmetry, except that  $G(z)$  is replaced by  $G(z) \cos^2 \Theta(z)$ . Using the convention of Montagner & Nataf (1988), who define the tilt of the axis from the vertical direction, we set

$$x = \cos(2\Theta_1), \tag{28}$$

where  $\Theta_1 = \pi/2 - \Theta$ .

By projecting the transverse component on  $\dot{u}_R$ , and after replacing in eq. (27) the summation over layers by integrals over depth, we obtain

$$\begin{aligned}
\int \frac{G(z)}{2V_S L(z)} (1-x) \sin 2\Psi_G dz &= \sin 2\hat{\Psi} \frac{\delta \hat{t}}{2} \cos^2 \hat{\Theta}, \\
\int \frac{G(z)}{2V_S L(z)} (1-x) \cos 2\Psi_G dz &= \cos 2\hat{\Psi} \frac{\delta \hat{t}}{2} \cos^2 \hat{\Theta},
\end{aligned} \tag{29}$$

and

$$\int \frac{G(z)}{2V_S L(z)} \sqrt{(1-x^2)} \sin \Psi_G dz = \sin 2\hat{\Theta} \frac{\delta \hat{t}}{2} \sin \hat{\Psi},$$

$$\int \frac{G(z)}{2V_S L(z)} \sqrt{(1-x^2)} \cos \Psi_G dz = \sin 2\hat{\Theta} \frac{\delta \hat{t}}{2} \cos \hat{\Psi}, \quad (30)$$

where we have defined effective fast axis azimuth  $\hat{\Psi}$  and effective timed lay  $\delta \hat{t}$  as previously, and introduced an effective tilt angle  $\hat{\Theta}$ . The products on the right-hand side of eqs (29) and (30) can be obtained from the expansions in  $\cos n\Psi$  of the two projections, that is, from the ‘splitting intensity’, as defined by Chevrot (2000), consisting in projecting the  $u_T$  component onto the time derivative of radial component  $\dot{u}_R$ . Indeed, assuming  $u_T^0 = 0$ , to first order, the expression for the splitting intensity (SI) is

$$\text{SI} = \left[ \sum_{j=0}^n \frac{\delta t_j}{2} [\cos^2 \Theta_j \sin 2\Psi'_j + \sin 2\Theta_j \sin \Psi'_j \tan I] \right] \dot{u}_R^0 \quad (31)$$

or, for an equivalent one layer

$$\text{SI} = \frac{\delta \hat{t}}{2} [\cos^2 \hat{\Theta} \sin 2(\hat{\Psi} - \Psi) + \sin 2\hat{\Theta} \sin(\hat{\Psi} - \Psi) \tan I] \dot{u}_R^0, \quad (32)$$

and the coefficients of the harmonic terms in  $2\Psi$  and  $\Psi$  give the desired quantities on the right-hand side of eqs (29) and (30).

In practice, both vertical and radial components need to have sufficient signal-to-noise ratio, which can only be achieved if the incidence angle  $I$  is sufficiently large. While this condition is not met for quasi-vertically incident *SKS* waves, it is appropriate for teleseismic *S* waves and *Ps* converted phases.

In Fig. 7, we illustrate the effect of a tilted fast axis of anisotropy on the splitting intensity, in the case of a single anisotropic layer. Synthetics are computed at a period of 8 s as previously. The decomposition of the splitting intensity into its Fourier components in  $\Psi$  and  $2\Psi$  provides estimates of the quantities in the right-hand side of eqs (29) and (30). The splitting intensity is measured in two ways: first from the projection of the transverse component onto the time derivative of the radial component as a function of azimuth (Chevrot 2000), and second, by directly searching for the three parameters  $\hat{\theta}$ ,  $\hat{\Psi}$  and  $\delta \hat{t}$  using the cross-convolution method of Menke & Levin (2003), generalized to the simultaneous search for  $\hat{\theta}$  (Yuan *et al.* 2008). We see that the results obtained by the two methods are in good agreement. Also, the effective parameters above are retrieved accurately, in the theoretical case where the data are uniformly distributed with azimuth. Fig. 7 illustrates the progressive loss of  $180^\circ$  periodicity as the tilt angle  $\hat{\theta}$  increases, due to the increasing influence of the second term in the right-hand side of eq. (32).

In Fig. 8, we present the splitting intensity measured in the case of two anisotropic layers. The models are similar to models A and B in Fig. 3 (with different orders of layers) except that we have added a dip of  $30^\circ$  along the fast direction. Again, synthetics are computed for the two models as previously at 8 s, and the splitting intensity is measured in two fashions, yielding comparable results. We see the influence of the  $1-\Psi$  term in eq. (31) which breaks the  $180^\circ$  periodicity in the splitting intensity. Again, from the splitting intensity measurements, or from the direct search for the effective anisotropic parameters, we can obtain the right-hand side of eqs (29) and (30). The measured angles are within  $5^\circ$  of those in the input models, which is within the uncertainty of any measurements on real data.

Eqs (29) and (30) can then be combined with constraints from surface waveforms to invert not only for the azimuth of the fast

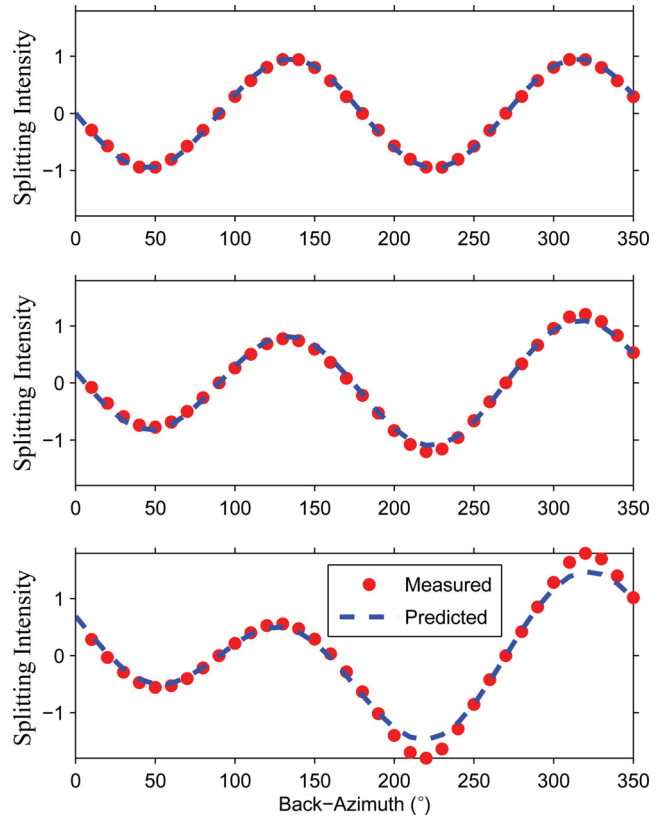


**Figure 7.** Splitting intensity measurements and predictions for one-layer cases. The synthetic models have a single anisotropic layer, with splitting time  $\delta t = 1.27$  s, horizontal fast axis direction  $\Psi = \text{N}90^\circ\text{E}$ , and different dipping axis angles  $\theta = 0^\circ, 10^\circ$  and  $30^\circ$  for the top, middle and bottom panels, respectively. The splitting intensity (Chevrot 2000; red dots) is measured from synthetic *T* and *R* waveforms computed with an anisotropic reflectivity code (Park 1996; Park & Levin 1997) at a period of 8 s. The predicted splitting intensity values (eq. 32), are computed using the one-layer equivalent apparent splitting parameters  $\hat{\Psi}$ ,  $\delta \hat{t}$  and  $\hat{\theta}$  measured with the cross-convolution method (Menke & Levin 2003; Yuan *et al.* 2008). The incidence angle  $I$  of the input *SV* wave is  $10^\circ$  in all computations. Note that the measured splitting intensity generally matches the analytic prediction very well for all models, and that including a dipping fast axis (middle and bottom panels) breaks the  $180^\circ$  periodic pattern of the splitting intensity, present only in the case with horizontal fast axis direction (top panel).

axis direction as a function of depth, but also for the tilt of the anisotropic axis of symmetry (Montagner & Nataf 1988), which may be possible at least in some depth domains of the upper mantle, and for stations with sufficient azimuthal coverage. The tilt of the anisotropic axis of symmetry is generally difficult to constrain from surface wave measurements alone.

#### 4 DISCUSSION AND CONCLUSIONS

We have shown that the observed quantities used in the joint inversion of *SKS* splitting measurements and surface waveforms (e.g. Marone & Romanowicz 2007; Yuan & Romanowicz 2010) are station-averaged estimates of splitting time and fast axis direction that do not depend on the order of anisotropic layers to second order in the small quantity  $\omega \delta t$ . They can be retrieved from *SKS* data in the frequency range where most splitting measurements are made (8–15 s). In contrast, measurements of splitting at single azimuths depend on the order of anisotropic layers as shown by Silver & Savage (1994) and Silver & Long (2011). We show here that

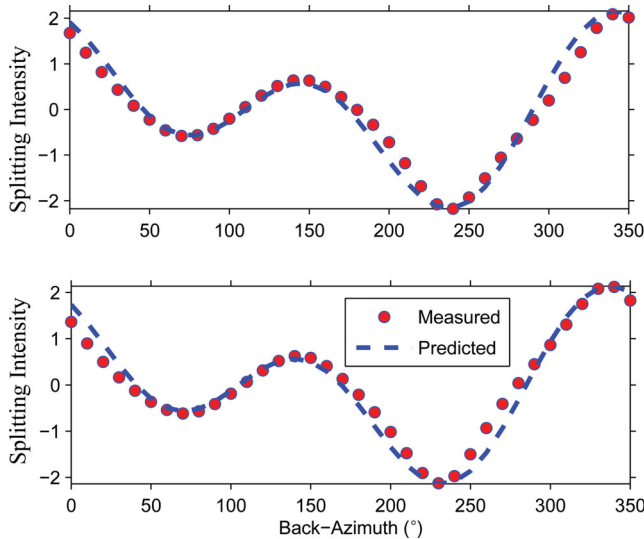


**Figure 8.** Splitting intensity measurements and predictions for two-layer models. The synthetic models are modified from Model A (top panel) and B (bottom panel) in Table 1, adding a dip of  $\theta = 30^\circ$  in each layer has  $30^\circ$  dip along the horizontal fast axis direction. Red dots represent measured splitting intensity obtained by projecting the  $T$  component onto the time derivative of the  $R$  component. The equivalent apparent splitting parameters for computing the predicted splitting intensity (eq. 32) are  $\Psi = -70^\circ$ ,  $\delta t = 2.03$  and  $\hat{\theta} = 37^\circ$  for the top model and  $\Psi = -75^\circ$ ,  $\delta t = 2.03$  s and  $\hat{\theta} = 37^\circ$ , for the bottom model. The incidence angle of the input  $SV$  wave is  $30^\circ$  in all computations to illustrate the  $360^\circ$  periodicity in the splitting intensity contributed by the  $\sin\Psi$  and  $\cos\Psi$  terms in eq. (26). The measured splitting intensity matches the analytic predictions very well in both cases, and is independent of the order of anisotropic layers.

such measurements may be unreliable, because their interpretation involves divisions by quantities that can become very small.

Until now, the joint inversion of splitting and surface waveform data has been performed under the assumption of horizontal fast axis of anisotropy. However, it is important to try and constrain the variations in the dip of the fast axis of anisotropy in the upper mantle, to better understand the present and past dynamics in various tectonic settings. In particular, radial anisotropy is known to be weaker in the continental upper mantle than under the oceans (e.g. Babuska *et al.* 1998), and azimuthal anisotropy is weaker in the continental lithosphere than in the underlying asthenosphere (e.g. Yuan *et al.* 2011). This may indicate either absence of strong anisotropy or a significant tilt of the fast axis in the continental lithosphere (e.g. Gaherty 2004). Resolving this may help understand the circumstances under which frozen anisotropy in the lithosphere was formed.

We have shown here that the relations obtained by MGL00 and applied by us in joint inversions of SKS splitting measurements and surface waveforms can be extended to the case of a tilted axis (or a series of layers with different tilts), and that information on the tilt can be obtained in a similar way to the case of a horizontal axis of symmetry, also by considering quantities derived from station-averaged measurements. Combined with surface waveforms, this may lead to improved constraints on the tilt of the fast axis as a function of depth.

These station-averaged, ‘effective’ parameters can be obtained from observations in several different ways. One way is from the measurement of the ‘splitting intensity’ as defined by Chevrot (2000). Indeed, if the tilt of the fast axis is significant and the inci-

dence angle of the  $S$  wave at the bottom of the anisotropic layer stack is large enough, the splitting intensity contains azimuthal components in both  $2\Psi$  and  $1\Psi$ , which together allow us to constrain not only the effective splitting time and fast axis direction, but also the effective tilt. Eqs (31) and (32) give simple analytical expressions for the splitting intensity valid for flat and dipping layers. Alternatively, it is also possible to retrieve these three effective parameters through a parameter search, extending the cross-convolution method of Menke & Levin (2003) to the case of tilted fast axis (Yuan *et al.* 2008). Both methods use measurements at all available azimuths, therefore should yield robust results if the azimuthal coverage is adequate to resolve both  $2\Psi$  and  $1\Psi$  harmonic components in azimuth. A systematic analysis of existing splitting data at the global scale for breaks in the  $180^\circ$  periodicity of the splitting intensity would provide a way to detect the presence of significant fast axis tilts.

In practice, observational conditions will not be perfect. Data are often noisy, and the azimuthal distribution around most stations is far from uniform. Moreover, the incidence angle  $I$  at the bottom of the stack of anisotropic layers will not be quite constant with azimuth. This will introduce some scatter around the theoretical splitting intensity curves, and a careful choice of epicentral distances around each station will be necessary. Practical applications and their challenges are beyond the scope of this paper. However, the results presented here provide a framework for the extension of the joint inversion of surface waveforms and SKS splitting data to include  $S$  and  $Ps$  conversion data in a forthcoming paper. We note that efforts at extracting anisotropy from  $Ps$  conversion data using receiver function analysis have been documented (e.g. Levin & Park 2000; Park & Levin 2002).

The derivations presented here have been conducted in the framework of ray theory, but could be extended to the case of finite frequency kernels (i.e. Chevrot 2006) in a straightforward manner. Finally, we note that the expressions derived here as an extension to the work of MGL00 are only valid, strictly speaking, under the assumption that the dependence of anisotropy on azimuth can be described by terms up to  $2\Psi$  only, and that the terms in  $4\Psi$  can be neglected. Such additional terms arise in the general expressions for the azimuthal dependence of Love-wave velocities and the  $SH$  component of body waves. This may not be accurate in some parts of the upper mantle (e.g. Becker *et al.* 2006). Because we are projecting on the Fourier components of  $\Psi$ , we do not need to worry about the  $4\Psi$  terms that would arise in the general case in eqs (24)–(26), as long as the  $1\Psi$  and  $2\Psi$  terms can be measured accurately. This, in practice, is more realistic than going after  $4\Psi$  terms, given the generally insufficient azimuthal sampling by available data. In particular, the presence of a significant  $1\Psi$  term is diagnostic of the presence of a dip in the fast axis direction (e.g. Montéiller & Chevrot 2010), and it is therefore of interest to determine and try and interpret this term. While the  $1\Psi$  and  $2\Psi$  coefficients terms can perhaps be measured accurately, their interpretation, in the general case, will include additional terms that depend on the tilt of the axis  $\Psi$ . Indeed, in eqs (24)–(30) we have made the assumption that non-linear terms in  $x = \cos(2\Psi)$ , as derived in Montagner & Nataf (1988), eq. (14) in that paper, can be neglected, which corresponds to the case of ‘elliptical anisotropy’ as defined in Levin & Park (1998) and Becker *et al.* (2006). Quantification of the error on the corresponding tilt in the fast axis of anisotropy, due to the simplified assumptions made, depends on the specific model of anisotropy chosen and is beyond the scope of this paper. We note that Chevrot (2006) derived exact expressions for splitting intensities in the presence of a tilted axis of symmetry and oblique incidence, which could be used, in

combination with the expressions of Montagner & Nataf (1988), as a starting point to further generalize eqs (29) and (30).

## ACKNOWLEDGMENTS

We thank Kelly H. Liu and Derek L. Schutt for sharing their SKS waveforms, and Sebastien Chevrot and Editor Jeannot Trampert for their constructive reviews. This is the BSL contribution 11-7. This work was partially supported by NSF EAR grant # 0738284.

## REFERENCES

- Anderson, D.L., 1961. Elastic wave propagation in layered anisotropic media, *J. geophys. Res.*, **66**, 2953–2963.
- Babuska, V., Montagner, J.P., Plomerov, J. & Girardin, N., 1998. Age-dependent large-scale fabric of the mantle lithosphere as derived from surface-wave velocity anisotropy, *Pure appl. Geophys.*, **151**, 257–280.
- Becker, T., Chevrot, S., Schulte-Pelkum, V. & Blackman, D., 2006. Statistical properties of seismic anisotropy predicted by upper mantle geodynamic models, *J. geophys. Res.*, **111**, B08309, doi:10.1029/2005JB004095.
- Chevrot, S., 2000. Multichannel analysis of shear wave splitting, *J. geophys. Res.*, **105**, 21 579–521 590.
- Chevrot, S., 2006. Finite-frequency vectorial tomography: a new method for high-resolution imaging of upper mantle anisotropy, *Geophys. J. Int.*, **165**, 641–657.
- Chevrot, S. & van der Hilst, R.D., 2003. On the effects of a dipping axis of symmetry on shear wave splitting measurements in a transversely isotropic medium, *Geophys. J. Int.*, **152**, 497–505.
- Debayle, E. & Kennett, B.L.N., 2000. Anisotropy in the Australasian upper mantle from Love and Rayleigh waveform inversion, *Earth planet. Sci. Lett.*, **184**, 339–351.
- Debayle, E., Kennett, B. & Priestley, K., 2005. Global azimuthal seismic anisotropy and the unique plate-motion deformation of Australia, *Nature*, **433**, 509–512.
- Dziewonski, A.M. & Anderson, D.L., 1981. Preliminary reference Earth model, *Phys. Earth planet. Inter.*, **25**, 297–356.
- Ekström, G. & Dziewonski, A.M., 1998. The unique anisotropy of the Pacific upper mantle, *Nature*, **394**, 168–172.
- Forsyth, D.W., 1975. The early structural evolution and anisotropy of the oceanic upper mantle, *Geophys. J. R. astr. Soc.*, **43**, 103–162.
- Gaherty, J.B., 2004. A surface wave analysis of seismic anisotropy beneath eastern North America, *Geophys. J. Int.*, **158**, 1053–1066.
- Gripp, A.E. & Gordon, R.G., 2002. Young tracks of hotspots and current plate velocities, *Geophys. J. Int.*, **150**, 321–361.
- Gung, Y., Panning, M. & Romanowicz, B., 2003. Global anisotropy and the thickness of continents, *Nature*, **422**, 707–711.
- Hess, H.H., 1964. Seismic anisotropy of the uppermost mantle under oceans, *Nature*, **203**, 629–631.
- Levin, V. & Park, J., 1997. P-SH conversions in a flat-layered medium with anisotropy of arbitrary orientation, *Geophys. J. Int.*, **131**, 253–266.
- Levin, V. & Park, J., 1998. P-SH conversions in layered media with hexagonally symmetric anisotropy: a cookbook, *Pure appl. Geophys.*, **151**, 669–697.
- Levin, V. & Park, J., 2000. Shear zones in the Proterozoic lithosphere of the Arabian Shield and the nature of the Hales discontinuity, *Tectonophysics*, **323**, 131–148.
- Liu, K.H., 2009. NA-SWS-1.1: A uniform database of teleseismic shear wave splitting measurements for North America, *Geochem. Geophys. Geosyst.*, **10**, doi:10.1029/2009gc002440.
- Love, A.E.H., 1911. *Some Problems of Geodynamics*, Cambridge University Press, Cambridge, UK.
- Marone, F. & Romanowicz, B., 2007. The depth distribution of azimuthal anisotropy in the continental upper mantle, *Nature*, **447**, 198–201.
- Marone, F., Gung, Y. & Romanowicz, B., 2007. 3D radial anisotropic structure of the North American upper mantle from inversion of surface waveform data, *Geophys. J. Int.*, **171**, 206–222, doi:10.1111/j.1365-246X.2007.03456.
- Menke, W. & Levin, V., 2003. The cross-convolution method for interpreting SKS splitting observations, with application to one and two-layer anisotropic earth models, *Geophys. J. Int.*, **154**, 379–392.
- Montagner, J.-P., 2002. Upper mantle low anisotropy channels below the Pacific plate, *Earth planet. Sci. Lett.*, **202**, 263–274.
- Montagner, J.-P. & Nataf, H.-C., 1986. A simple method for inverting the azimuthal anisotropy of surface waves, *J. geophys. Res.*, **91**, 511–520.
- Montagner, J.-P. & Nataf, H.-C., 1988. Vectorial tomography I. Theory, *Geophys. J. R. astr. Soc.*, **94**, 295–307.
- Montagner, J.-P. & Tanimoto, T., 1991. Global upper mantle tomography of seismic velocities and anisotropies, *J. geophys. Res.*, **96**, 20 337–20 351.
- Montagner, J.-P., Griot-Pommere, D.-A. & Lave, J., 2000. How to relate body wave and surface wave anisotropy? *J. geophys. Res.*, **105**, 19 915–19 027.
- Monteiller, V. & Chevrot, S., 2010. How to make robust splitting measurements for single-station analysis and three-dimensional imaging of seismic anisotropy, *Geophys. J. Int.*, **182**, 311–328.
- Nataf, H.-C., Nakanishi, I. & Anderson, D.L., 1986. Measurements of mantle wave velocities and inversion for lateral heterogeneities and anisotropy 3. Inversion, *J. geophys. Res.*, **91**, 7261–7307.
- Park, J., 1996. Surface waves in layered anisotropic structures, *Geophys. J. Int.*, **126**, 173–183.
- Park, J. & Levin, V., 2002. Seismic anisotropy: tracing plate dynamics in the mantle, *Science*, **296**, 485–489, doi:10.1126/science.1067319.
- Rümpker, G. & Silver, P.G., 1998. Apparent shear-wave splitting parameters in the presence of vertically varying anisotropy, *Geophys. J. Int.*, **135**, 790–800.
- Saltzer, R.L., Gaherty, J.B. & Jordan, T.H., 2000. How are vertical shear wave splitting measurements affected by variations in the orientation of azimuthal anisotropy with depth?, *Geophys. J. Int.*, **141**, 374–390.
- Schlue, J.W. & Knopoff, L., 1977. Shear-wave polarization anisotropy in the Pacific Basin, *Geophys. J. R. astr. Soc.*, **49**, 145–165.
- Silver, P.G., 1996. Seismic anisotropy beneath the continents: probing the depths of geology, *Annu. Rev. Earth planet. Sci.*, **24**, 385–432.
- Silver, P.G. & Chan, W.W., 1991. Shear wave splitting and subcontinental mantle deformation, *J. geophys. Res.*, **96**, 16 429–16 454.
- Silver, P.G. & Long, M.D., 2011. The non-commutivity of shear wave splitting operators at low frequencies and implications for anisotropy tomography, *Geophys. J. Int.*, **184**, 1415–1427.
- Silver, P.G. & Savage, M.K., 1994. The interpretation of shear-wave splitting parameters in the presence of two anisotropic layers, *Geophys. J. Int.*, **119**, 949–963.
- Simons, F.J., van der Hilst, R.D., Montagner, J.P. & Zielhuis, A., 2002. Multi-mode Rayleigh wave inversion for heterogeneity and azimuthal anisotropy of the Australian upper mantle, *Geophys. J. Int.*, **151**, 738–754.
- Smith, M.L. & Dahlen, F.A., 1973. The azimuthal dependence of Love and Rayleigh wave propagation in a slightly anisotropic medium, *J. geophys. Res.*, **78**, 3321–3333.
- Smith, D., Ritzwoller, M.H. & Shapiro, N., 2004. Stratification of anisotropy in the Pacific upper mantle, *J. geophys. Res.*, **109**, doi:10.1029/2004JB003200.
- Vinnik, L.P., Farra, V. & Romanowicz, B., 1989. Azimuthal anisotropy in the Earth from observations of SKS at GEOSCOPE and NARS broadband stations, *Bull. seism. Soc. Am.*, **79**, 1542–1558.
- Yuan, H. & Romanowicz, B., 2010. Lithospheric layering in the North American craton, *Nature*, **466**, 1063–1068.
- Yuan, H., Ducker, K. & Schutt, D., 2008. Testing five of the simplest upper mantle anisotropic velocity parameterizations using teleseismic S and SKS data from the Billings, Montana PASSCAL array, *J. geophys. Res.*, **113**, doi:10.1029/2007JB005092.
- Yuan, H., Romanowicz, B., Fischer, K.M. & Abt, D., 2011. 3-D shear wave radially and azimuthally anisotropic velocity model of the North American upper mantle, *Geophys. J. Int.*, **184**, 1237–1260.